THE JOURNAL OF PHYSICAL CHEMISTRY LETTERS
A JOURNAL OF THE AMERICAN CHEMICAL SOCIETY

pubs.acs.org/JPCL

Letter

Polaron-Induced Midgap States in Ovonic Threshold Switching Material for 3D Phase-Change Memory Applications

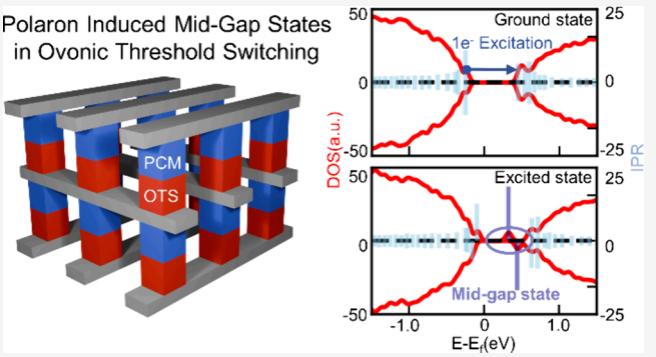
Huan-Ran Ding, Tian-Yu Zhao, Nian-Ke Chen,* Bai-Qian Wang, Shun-Yao Qin, Meng Niu, Si-Bo Wang, Yu-Ting Huang, Ming Xu, and Xian-Bin Li*

Cite This: J. Phys. Chem. Lett. 2026, 17, 2213−2221

Read Online

ACCESS | Metrics & More | Article Recommendations | Supporting Information

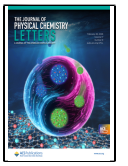
ABSTRACT: Ovonic threshold switching (OTS)-based selector is essential for suppressing sneak-path current in 3D-crossbar phase-change memory. Although midgap (defect) states of OTS amorphous materials are crucial for the switching process, their origin and evolution remain insufficiently understood, and elucidating their governing mechanism is essential for resolving debates on OTS behavior. Here, first-principles calculations investigate the electron−hole-pair excitation during the switching-on process in three representative OTS materials—GeSe, GeS, and SiGeAsTe. The results reveal that excited carriers (electron−hole-pairs) induce polaron formation through strong electron−phonon coupling. Polarons introduce midgap states that could promote the switching-on process through positive feedback. Further analyses demonstrate that the polarons and midgap states are mainly related to the conduction band. This is attributed to the unique metavalent bonding or hyperbonding effects in chalcogenide OTS materials. These findings clarify the formation of midgap states from excited-state and polaron perspectives, and provide guidance for designing improved OTS materials for 3D phase-change memory.



To meet the growing demands for high-performance, high-density, and low-power nonvolatile memory (NVM), three-dimensional (3D) stacking architectures have emerged as a key direction in development of memory integrated circuits (IC). By vertically stacking memory cells with peripheral circuits, 3D NVM greatly boosts storage density. However, as technology nodes continue to scale down and the number of stacked layers grows, the resistance and capacitance of metal interconnects also increase, which leads to more crosstalk and more severe leakage current problems. For example, in 3D phase-change memory, leakage current not only reduces the read/write speed and risks data integrity but also causes data retention failures, higher power consumption, and shorter device lifespan.[1,2] To address these issues, one of the most effective architectural strategies is stacking a selector device for each memory cell, creating a cross-point memory array (Figure 1a).[3] The selector device must display nonlinear conduction properties to suppress leakage current from unselected cells while ensuring reliable read/write functions at high voltage levels.

A variety of selectors have been proposed, including ovonic threshold switching (OTS),[4] mixed ion-electron conductor (MIEC),[5] metal−insulator transition (MIT),[6] and ion-diffusion threshold switching,[7] as well as several other types. Among these selectors, OTS devices based on chalcogenide amorphous materials are highly promising due to their high on-state driving current (>10 MA/cm^2), fast switching speed, and excellent endurance.[8] OTS has been reported in a variety of amorphous chalcogenide materials. Representative OTS materials include S-based, Se-based, and Te-based chalcogenide systems, such as GeS,[9] Ge−As−S,[10] GeSe,[11] Ge−As−Se,[12] and SiGeAsTe,[13] which are characterized by stable amorphous networks, strong electronic localization, and pronounced nonlinear electrical conductivity. These features make them suitable for reliable threshold switching. In recent years, a novel memory device known as selector-only memory (SOM) (Figure 1b), based solely on OTS devices, has also attracted significant attention.[14] The unique feature of SOM devices lies in their ability to induce reversible changes in the OTS threshold voltage by modulating the polarity of the applied voltage, thereby enabling nonvolatile data storage. Specifically, the typical $I-V$ characteristics of OTS devices exhibit pronounced nonlinearity (Figure 1c).[3] When the applied voltage is below the threshold voltage (V_{th}), the

Received: November 10, 2025
Revised: January 24, 2026
Accepted: February 9, 2026
Published: February 13, 2026



Downloaded from pubs.acs.org/jpclcd/article-pdf/17/8/2213/6319089/jz5c03532.pdf by JILIN UNIV, Yu-Ting Huang on 28 October 2026

© 2026 American Chemical Society

https://doi.org/10.1021/acs.jpclett.5c03532
J. Phys. Chem. Lett. 2026, 17, 2213−2221

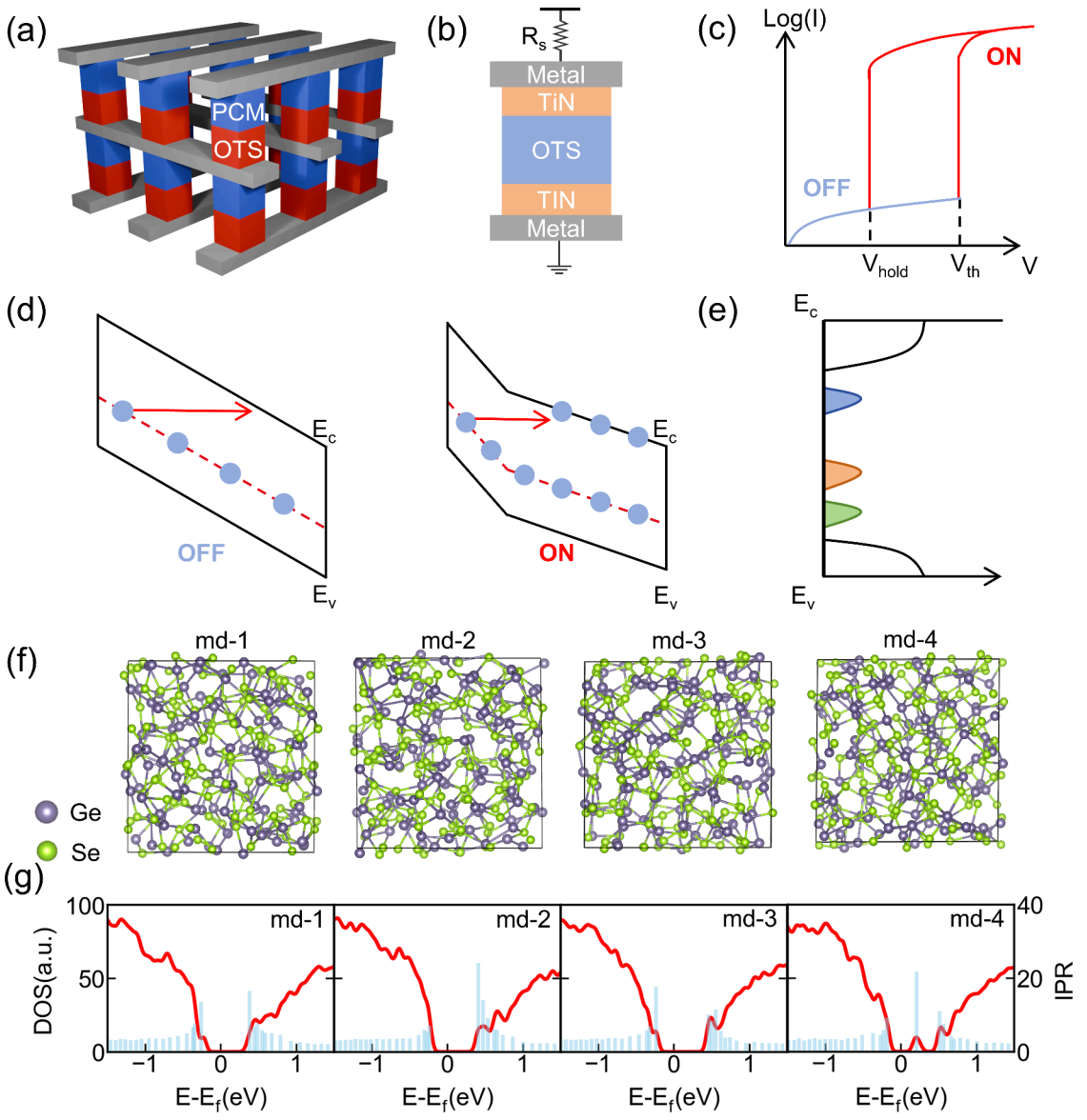


Figure 1. (a) Schematic picture of the 3D Crosspoint architecture. The blue and red blocks indicate the memory and selector cells, respectively. (b) Device structure of a selector-only memory. (c) Schematic picture of the typical current−voltage (I−V) curves of OTS selectors. The device remains in a high-resistance state (OFF) at zero or low bias. Once the voltage reaches the threshold voltage (V_{th}), the current increases sharply and the device switches to a low-resistance state (ON). When the voltage drops below the holding voltage (V_{hold}), the device switches off. (d) Schematic illustration of the Poole−Frenkel emission mechanism of OTS, where the electric field will bend the energy band, leading to carriers hopping from defect states to shallow energy states or conduction bands, thus turning on the device. (e) Schematic of the midgap states in the density of states of OTS materials. Generally, an ideal OTS material should contain sufficient midgap states within the band gap. (f) Snapshots of the structures of amorphous GeSe obtained by four different melt-quench simulations. Purple and green balls indicate Ge and Se atoms, respectively. (g) Density of states of the four models of amorphous GeSe. The red curve represents the density of states, and the blue lines represent the IPR. The larger the value of IPR, the more localized the electronic state is.

device remains in a high-resistance state (OFF). Once the voltage exceeds V_{th}, the current increases sharply, and the device transitions to a low-resistance state (ON). When the voltage drops below the holding voltage (V_{hold}), the device switches off and reverts to the high-resistance state. This fast and reversible switching behavior positions OTS devices as highly promising candidates for selector applications.

Although OTS devices exhibit excellent electrical performance, their underlying physical mechanisms are still not fully understood.[15−26] Among the various switching mechanisms proposed, a high-field Poole−Frenkel (PF) transport threshold switching model based on midgap states (or called defect states) within the band gap, first introduced by Ielmini et al.,[17] has gained widespread acceptance. Figure 1d shows the schematic picture of the midgap states-assisted transport mechanism, where the existence of such midgap states is crucial. To ensure efficient conduction, an ideal OTS material is, in principle, expected to contain a high density of midgap states within the band gap, as shown in Figure 1e. As such, midgap states are often used to elucidate the mechanism and evaluate the performance of OTS materials,[10,27] serve as key parameters in analytical models,[17,28] and act as descriptors for screening potential OTS materials.[29] For ground state, the origin of the midgap states has been attributed to over/under-

https://doi.org/10.1021/acs.jpclett.5c03532
J. Phys. Chem. Lett. 2026, 17, 2213−2221

Downloaded from pubs.acs.org/jpclcd/article-pdf/17/8/2213/6319089/jz5c03532.pdf by JILIN UNIV, Yu-Ting Huang on 28 October 2026

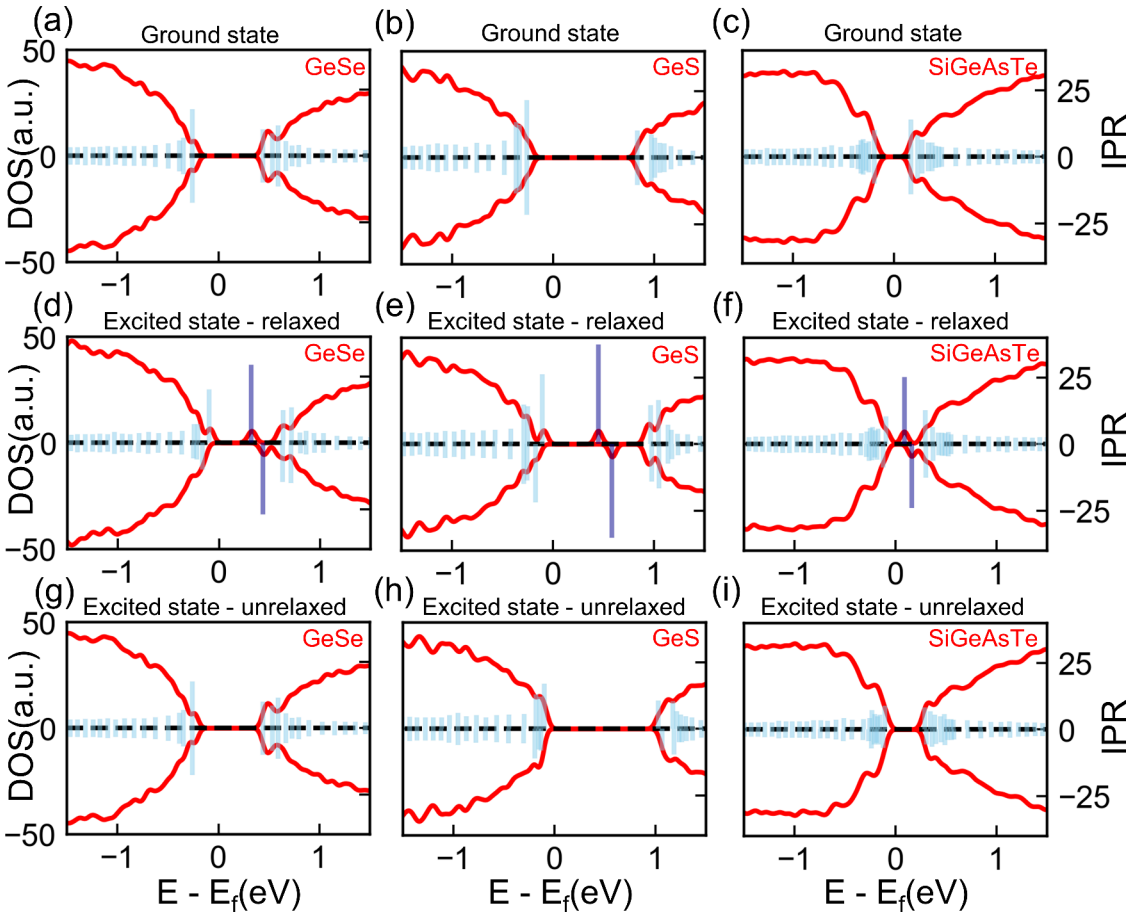


Figure 2. Spin-polarized density of states (DOS) of (a–c) ground state, (d–i) excited state with structural relaxations and (g–i) excited state without structural relaxations for a-GeSe, a-GeS, and a-SiGeAsTe, respectively. The red curve represents the density of states, and the blue lines represent the IPR. The dark blue IPR indicates a newly generated midgap state.

coordinated atoms (valence-alternation pairs model) in amorphous Ge_xSe_y,[30] Ge–Ge bonds or Ge–Ge chains in amorphous GeTe.[31] Xu et al. found that medium-range order that breaks the global 8–N rule also produces midgap states, which pioneers the integration of machine learning with first-principles modeling to decode the structural origins of midgap states in chalcogenide glasses, offering a transformative strategy for accelerating the design of high-performance ovonic threshold switching materials and advancing next-generation memory integration.[32] However, previous studies indicate that most computationally generated amorphous models possess few midgap states; notably, approximately 60% of amorphous GST models have been reported to exhibit no such states.[26,32,33] This phenomenon has been attributed to the tendency of chalcogenide glasses to form lone pairs and eliminate dangling bonds, resulting in a relatively clean band gap.[34,35] It was also found that the hypervalent bonding delocalizes the defect electrons and suppresses the formation of midgap states, which provides a critical physical insight into the role of special bonding in tailoring midgap states of chalcogenide glass, paving a novel pressure-inspired pathway for the rational design of high-performance phase-change and ovonic threshold switching materials.[36] Moreover, recent research found that a strong electric field can reduce the density of the midgap states in amorphous phase-change memory (PCM) materials and even eliminate them.[37] The charged-state transition of the traps was also found can enhance the localization of the trap states.[38] These findings suggest that the density of the midgap states is not constant but can change during the switching process. The evolution of midgap states during device operation still requires further clarification, as it is crucial for a deeper understanding of the mechanism underlying OTS behavior.

In this work, using three typical OTS materials, including a-GeSe, a-GeS, and a-SiGeAsTe (where the prefix "a-" denotes amorphous), as examples, first-principles calculations found that electron–hole pairs which could be generated during the device operation process can form small polarons with local structural relaxations. The formation of polarons instantly introduces midgap states in these materials by altering the energy of the band-tail states. Moreover, these polarons are found to be mainly contributed by the coupling between local structures and electrons in conduction band. The reason is attributed to the unique metavalent or hyper bonds in chalcogenide glasses. The generation of midgap states via forming polarons will benefit the Poole–Frenkel emission and thus could provide positive feedback on the threshold switching process. The identification of polarons in OTS materials provides an atomic-level picture of the evolution of defect states during device operation, which offers insights to clarify the mechanism of OTS behaviors.

Calculations based on density-functional theory (DFT) were performed using the Vienna ab initio simulation package (VASP).[39–41] Projector augmented wave (PAW) pseudopo-

Downloaded from pubs.acs.org/jpclcd/article-pdf/17/8/2213/6319089/jz5c03532.pdf by JILIN UNIV, Yu-Ting Huang on 28 October 2026

https://doi.org/10.1021/acs.jpclett.5c03532
J. Phys. Chem. Lett. 2026, 17, 2213–2221

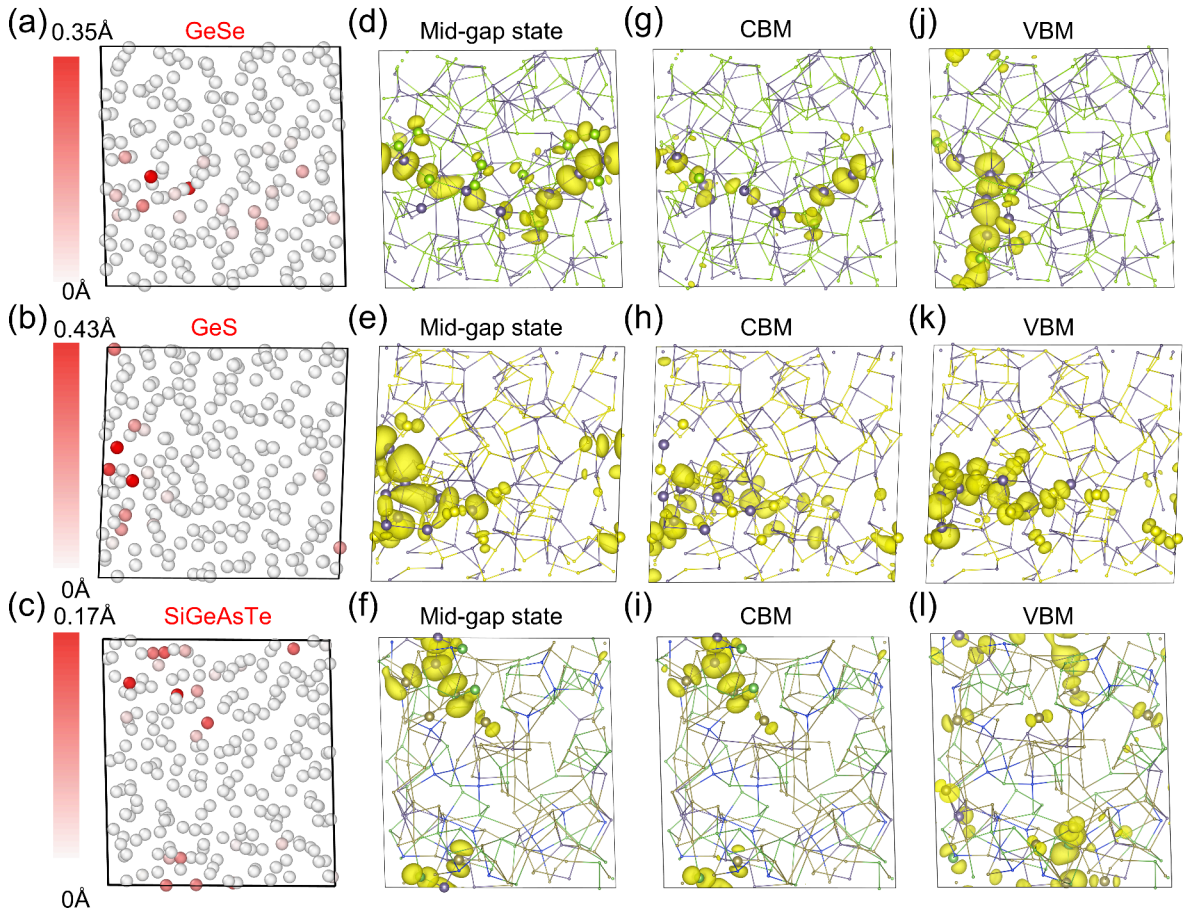


Figure 3. (a–c) Atomic displacement diagram of a-GeSe, a-GeS, and a-SiGeAsTe, respectively. The color indicates the displacements of each atom. Real-space projection of the (d–f) midgap state (g–i) CBM states and (j–l) VBM states for a-GeSe, a-GeS, and a-SiGeAsTe, respectively. The isosurface value for the projected charge density is 0.001 e/a_0^3, where a_0 is the Bohr radius.

tentials with generalized gradient approximation (GGA) exchange-correlation functional developed by Perdew, Burke, and Ernzerhof (PBE) were adopted.[42,43] The cutoff energy for plane-wave expansion was 400 eV for property evaluations and 300 eV for molecular dynamics (MD). The *k*-point grids for integration of the Brillouin zone were Monkhorst–Pack grid of 3 × 3 × 3 for property calculation and 1 × 1 × 1 (Γ point) for MD. MD simulations were performed using a time step of 3 fs within a canonical (NVT) ensemble. The models respectively contain 108 Ge and 108 Se atoms for GeSe, 108 Ge and 108 S atoms for GeS, and 22 Si, 22 Ge, 64 As and 108 Te atoms for SiGeAsTe. The reliability of the energy cutoff is further verified in Note 1 of the Supporting Information (SI). The relaxed dimensions of amorphous supercell models for electronic calculations are 17.83 Å × 18.00 Å × 17.98 Å for GeSe (here, using the md-3 model as an example), 18.11 Å × 17.37 Å × 17.85 Å for GeS, and 18.04 Å × 19.55 Å × 19.40 Å for SiGeAsTe, respectively. The liquid and amorphous models are obtained by the melt-quench method[44] with following steps: (1) the structure is fully diffused for 9 ps at a high temperature of 1500 K; (2) the liquid state was maintained at 1100 K for 9 ps; (3) the liquid at 1100 K is quenched to 300 K for 45 ps, and then the amorphous phase is maintained at 300 K for 9 ps. To verify the rationality of the amorphous models, the radial distribution functions (RDF) of the studied materials are calculated, which reasonably agree with previous reports (Note 2 and Figure S2 in the SI).[27,36] The density of state (DOS) and crystal orbital Hamilton population (COHP) were analyzed using the LOBSTER code.[45–47]

First, we performed four independent melt-quench processes by ab initio molecular dynamics (AIMD) simulations to obtain four different amorphous GeSe models (Figure 1f). The amorphous network of these models can be directly seen from the snapshots. Then, the density of states (DOS) and inversion participation ratio (IPR) of the four models are calculated (Figure 1g). The band gap of these amorphous materials can be observed. The localization of the electronic states in real space can be estimated by IPR.[48] A larger IPR value indicates a more localized state, whereas a smaller value corresponds to a more delocalized state. Figure 1g shows that, in all four models, the band-edge states are more localized than the in-band states, giving rise to Urbach tails in both the valence and conduction bands—a characteristic feature of amorphous materials. However, despite the obvious localized states at band edges, only one amorphous model (from md-4) has a midgap state. Using the same method, we also generated amorphous GeS,[27] and SiGeAsTe[49,50] for comparison (Figure 2a–c). Similarly, no midgap states are found in those amorphous models. These results are also consistent with previous studies.[32,33]

The concentration of carriers in OTS materials will significantly increase during the switching-on process. To mimic the effect of excited carriers (electron–hole pairs) in the switch-ON state, an electron is moved from the valence band maximum (VBM) to the conduction band minimum (CBM)

Downloaded from pubs.acs.org/jpclcd/article-pdf/17/8/2213/6319089/jz5c03532.pdf by JILIN UNIV, Yu-Ting Huang on 28 October 2026

https://doi.org/10.1021/acs.jpclett.5c03532
J. Phys. Chem. Lett. 2026, 17, 2213–2221

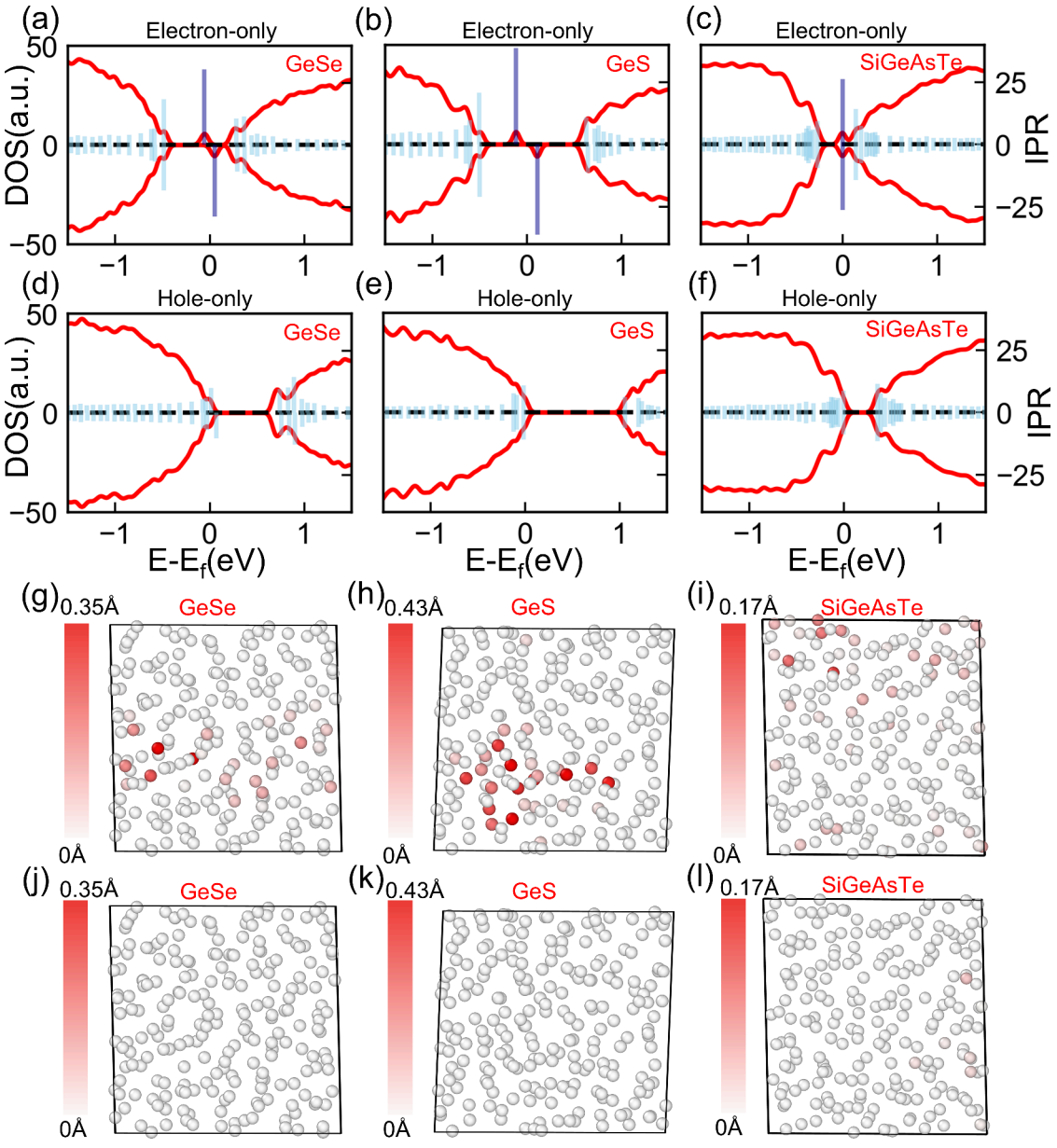


Figure 4. Total DOS of a-GeSe, a-GeS, and a-SiGeAsTe with (a–c) electron only doping and (d–f) hole only doping. It is clear that electrons produce midgap states. (g–l) Comparison of the atomic displacements of the two cases: (g–i) for the electron-only case and (j–l) for the hole-only case.

by fixing the electronic occupations.[51] Figure 2 compares the calculated spin-polarized DOS of these amorphous models before (Figure 2a–c) and after (Figure 2d–f) carrier excitations. Note that for the half-filled localized state, the spin polarization has been taken into account. For the ground states of the three amorphous models, no midgap states are observed in the DOS, whereas the IPR indicates localized band-edge states.

Note that hybrid HSE06 functional yields a similar tendency, i.e., the states near VBM and CBM are relatively localized while the in-band states are delocalized, as evidenced by the HSE06 DOS and IPR results (see Note 3 and Figure S4 in the SI). The charge density distributions at the VBM and CBM obtained from PBE and HSE06 are also qualitatively similar (Figures S5 and S6). After carrier excitation, midgap states emerge in the three kinds of OTS materials, indicating that this is a general effect rather than a coincidental occurrence. The IPR values of the emerged midgap states are very high, which is similar to the case of midgap states in the ground state (Figure 1g, md-4). Here, the atomic configuration at the final frame (9 ps) of the 300 K AIMD was selected for the electronic structure calculations. To ensure the reliability of the results, an additional configuration sampled at the 7.5 ps snapshot was also analyzed (see Note 2 and Figure S3 in the SI). The results, including the DOS, IPR, and polaron-induced midgap states, of the two snapshots agree reasonably with each other. Moreover, the electronic structures shown in Figure 2 are also recalculated using the meta-GGA SCAN functional (Figure S7 in the SI). The DOS under carrier excitation (with electron–hole pairs) obtained from SCAN functional clearly reproduce the emergence of midgap states, similar to the PBE results shown in Figure 2d–f. These results suggest that, during the switching-on process of the OTS materials, new midgap states will be generated due to the increase in carrier

https://doi.org/10.1021/acs.jpclett.5c03532
J. Phys. Chem. Lett. 2026, 17, 2213–2221

Downloaded from pubs.acs.org/jpclcd/article-pdf/17/8/2213/6319089/jz5c03532.pdf by JILIN UNIV, Yu-Ting Huang on 28 October 2026

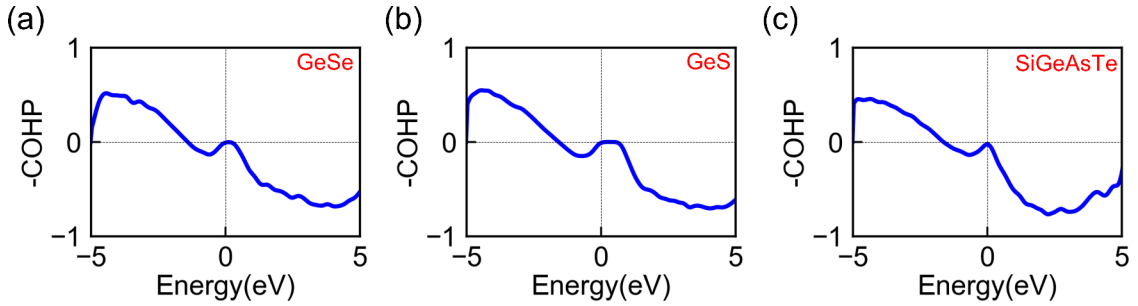


Figure 5. (a−c) The crystal orbital Hamilton population (COHP) of a-GeSe, a-GeS, and a-SiGeAsTe at the ground state, respectively.

concentration. Such an effect could possibly introduce positive feedback on the switching-on process of OTS materials, which is often omitted in analytic models.

The calculations in this work are performed without electric fields. Once electrons are excited to the conduction band minimum, electron polarons can form spontaneously, as the process can be realized by local relaxation governed by energy minimization. The electric field in OTS devices may indirectly influence polaron formation by regulating carrier excitations.

To elucidate the physical origin of the midgap states induced by electron−hole pairs, the spin-polarized DOS under excitation but without structural relaxation were also calculated in Figure 2g−i where no midgap states are observed. This significantly indicates that the emergence of midgap states arises primarily from electron−phonon like coupling rather than electron−electron interactions.

Figure 3a−c depicts the atomic displacements resulting from the carrier excitation-induced structural relaxations. The largest atomic displacements of a-GeSe, a-GeS, and a-SiGeAsTe are 0.35 Å, 0.43 Å and 0.17 Å, respectively. Such magnitudes of atomic displacements indicate that the electron−phonon coupling is indeed significant. Moreover, the sites of the most significant atomic displacements can be clearly identified from Figure 3a−c. Subsequently, the midgap states are projected into real space to examine their origins. Indeed, the locations of the midgap states closely coincide with the regions of atomic displacements. Therefore, it can be concluded that the midgap states in OTS materials originate from structural changes induced by carrier excitation. Such a carrier-induced structural relaxation is often referred to as a small polaron.[52−54] Note that the excitation-induced midgap states should be different from the intrinsic midgap states at ground state (such as the one in md-4 model of Figure 1g for a-GeSe). The intrinsic midgap state (or called defect state) is often attributed to the formation of Ge−Ge bonds or chains.[32] The location of the midgap state in md-4 indeed is related to the Ge−Ge chains (see Note 6 and Figure S9 in the SI). In contrast, here, the carrier-excitation-induced midgap states originate from strong electron−phonon coupling accompanied by local structural relaxations. This effect is robust, rather than being associated with pre-existing defect states (see Note 6 and Figure S9 in the SI).

To identify whether the midgap states are formed by the states from conduction band or valence band, the real-space projections of the midgap states (Figure 3d−f) are calculated and compared to the ones of the ground-state CBM (Figure 3g−i) and VBM (Figure 3j−l). The results reveal that the distribution of the midgap states is more like the ones of CBM states. In other words, the midgap states should mainly arise from the energy lowering of the CBM states via polaron formation, suggesting that they are electron polarons. Note that for GeS, the real-space distributions of the CBM and VBM states are similar.

To further verify the origin of the polaron effect, electron/hole-only doping is simulated by introducing an extra electron or hole (rather than an electron−hole pair) into the system. Figure 4a−f compare the calculated DOS of the two cases. The results show that adding electrons to the system indeed produces midgap states, while adding holes to the system does not cause a significant change in the DOS. The atomic displacements in Figure 4g−l also indicate that the electron doping results in significant structural changes. In contrast, the structural changes by hole doping are relatively small. In other words, the electron polaron effect is more significant. This may be attributed to the unique bonding feature of these materials,[55−58] see the further discussion below.

Figure 5 shows the crystal orbital Hamilton population (COHP) of the three OTS materials. It can be seen that both the top of the valence band and the bottom of the conduction band consist of antibonding states, which are generally energetically unfavorable for electron occupation. When the bottom of the conduction band is filled by electrons, the strong orbital interactions will lead to significant structural relaxations and thereby form small polarons. On the other hand, the antibonding states in the valence band can interact with lone-pair electrons to form metavalent or hyper bonds,[55−58] leading to electron sharing. Consequently, the loss of an electron in the VBM could be compensated by surrounding electrons, thereby preventing significant structural changes.

Since the midgap states mainly originate from electron polarons, the formation energy of polaron should be related to the position of the midgap states relative to CBM. Taking the results of carrier excitation (with electron−hole pairs) presented in Figures 2d−f as an example, we compare the positions of the trap states relative to CBM (ΔE_T) with the estimated formation energies of the polarons (ΔE_P) (see Note 5 in the SI for more details). Indeed, the values of ΔE_P are roughly comparable with ΔE_T (Table S1). In principle, the change in total energy after structural relaxation (ΔE_P) should consist of the energy change of the trap state (ΔE_T) and the energy changes of all other electronic orbitals influenced by the local structural relaxation ($\Delta E_T'$). For the amorphous materials studied in this work, the estimation is still relatively rough. Recently, a diagrammatic Monte Carlo approach based on first-principles electron−phonon coupling has been developed, which will more accurately calculate the polaron formation energies.[59] Further evaluations of polaron formation energies are worth pursuing in future work to achieve a deeper understanding on this issue.

Downloaded from pubs.acs.org/jpclcd/article-pdf/17/8/2213/6319089/jz5c03532.pdf by JILIN UNIV, Yu-Ting Huang on 28 October 2026

https://doi.org/10.1021/acs.jpclett.5c03532
J. Phys. Chem. Lett. 2026, 17, 2213−2221

The polarons in OTS materials should have substantial influences on the threshold switching of OTS devices. First, the formation of polarons results in more midgap states, which may facilitate the Poole−Frenkel emission. Then, the carrier excitation will possibly have positive feedback on the switching-on process. Second, the existence of polarons will lead to a low mobility of electrons and thus a low conductivity at relatively low temperatures. Therefore, the Joule heating effect during the holding process will gradually release these polarons and thereby enhance the mobility and conductivity. Such a contrast in electron mobility may enhance the ON/OFF ratio. According to a previous study,[60] when the concentration of the electrons reaches a critical value, the small polarons can also be released due to interactions between carriers, which has been considered as a mechanism of threshold switching. Moreover, the time required for polaron release may account for the limited speed (~ns) of the switch-OFF process after the voltage is removed. Therefore, the revealed polaron effect here will provide new clues to understanding the mechanism of OTS.[54,60,61]

In summary, first-principles calculations and molecular dynamics simulations reveal the carrier excitation induced polaron effect in three kinds of typical OTS materials including a-GeSe, a-Ge-S, and a-SiGeAsTe. The formation of polarons in OTS materials can induce midgap states due to strong electron−phonon coupling-induced local structure relaxations. The effect of electron polaron related to conduction band is significant. The midgap states are thus found to mainly originate from the energy lowering of the occupied CBM states. On one hand, the generation of midgap states would facilitate the threshold switching process via enhancing Poole-Frenkel emission. On the other hand, the formation of polarons should play an important role in modulating carrier mobility, which also contributes to the threshold switching process. Upon completion of the work, we learned that electron injection nearby the anode of a SOM device can lead to a similar polaronic effect which was used to explain the nonvolatile change of V_{th} in GeAsSe most recently.[62] In our work, we found that the polaron induced by excitation is volatile after de-excitation, possibly because only an electron−hole pair is considered in our simulations. The study provides new insights for understanding the working mechanism of OTS. We suggest that in the future the polaron effect should be taken into account when optimizing performances of OTS devices or designing new advanced OTS materials.

■ ASSOCIATED CONTENT

Data Availability Statement

All data need to evaluate the conclusions in the paper are present in the paper. All computational data are available from the authors upon reasonable request.

Supporting Information

The Supporting Information is available free of charge at https://pubs.acs.org/doi/10.1021/acs.jpclett.5c03532.

Supplemental tables and figures (PDF)

■ AUTHOR INFORMATION

Corresponding Authors

Nian-Ke Chen − *State Key Laboratory of Integrated Optoelectronics, College of Electronic Science and Engineering, Jilin University, 130012 Changchun, China*; Email: chennianke@jlu.edu.cn

Xian-Bin Li − *State Key Laboratory of Integrated Optoelectronics, College of Electronic Science and Engineering, Jilin University, 130012 Changchun, China*; orcid.org/0000-0002-0046-2016; Email: lixianbin@jlu.edu.cn

Authors

Huan-Ran Ding − *State Key Laboratory of Integrated Optoelectronics, College of Electronic Science and Engineering, Jilin University, 130012 Changchun, China*

Tian-Yu Zhao − *State Key Laboratory of Integrated Optoelectronics, College of Electronic Science and Engineering, Jilin University, 130012 Changchun, China*

Bai-Qian Wang − *State Key Laboratory of Integrated Optoelectronics, College of Electronic Science and Engineering, Jilin University, 130012 Changchun, China*

Shun-Yao Qin − *State Key Laboratory of Integrated Optoelectronics, College of Electronic Science and Engineering, Jilin University, 130012 Changchun, China*

Meng Niu − *State Key Laboratory of Integrated Optoelectronics, College of Electronic Science and Engineering, Jilin University, 130012 Changchun, China*

Si-Bo Wang − *State Key Laboratory of Integrated Optoelectronics, College of Electronic Science and Engineering, Jilin University, 130012 Changchun, China*

Yu-Ting Huang − *State Key Laboratory of Integrated Optoelectronics, College of Electronic Science and Engineering, Jilin University, 130012 Changchun, China*; orcid.org/0009-0005-9208-2780

Ming Xu − *School of Integrated Circuits, Huazhong University of Science and Technology, 430074 Wuhan, China*; orcid.org/0000-0002-2730-283X

Complete contact information is available at: https://pubs.acs.org/10.1021/acs.jpclett.5c03532

Author Contributions

Huan-Ran Ding: Formal analysis (lead); Investigation (lead); Software (lead); Writing − original draft (lead). **Tian-Yu Zhao:** Data curation (equal); Investigation (equal); Methodology (supporting). **Nian-Ke Chen:** Conceptualization (equal); Data curation (equal); Methodology (supporting); Supervision (lead); Writing − original draft (equal). **Bai-Qian Wang:** Formal analysis (supporting); Methodology (supporting). **Shun-Yao Qin:** Data curation (supporting); Methodology (supporting). **Meng Niu:** Investigation (supporting); Methodology (supporting). **Si-Bo Wang:** Formal analysis (supporting); Methodology (supporting). **Yu-Ting Huang:** Investigation (supporting); Methodology (supporting). **Ming Xu:** Methodology (supporting); Writing - review and editing (supporting). **Xian-Bin Li:** Conceptualization (equal); Funding acquisition (lead); Resources (lead); Supervision (lead); Writing − review and editing (equal).

Notes

The authors declare no competing financial interest.

■ ACKNOWLEDGMENTS

This work was supported by the National Science and Technology Major Project (Grant No. 2022ZD0117600), the National Natural Science Foundation of China (Grants No. 12274172, 12274180, 12504075), the Science and Technology Development Plan Project of Changchun, China (Grant No.

Downloaded from pubs.acs.org/jpclcd/article-pdf/17/8/2213/6319089/jz5c03532.pdf by JILIN UNIV, Yu-Ting Huang on 28 October 2026

2024GZZ07), and the Fundamental Research Funds for the Central Universities. The High-Performance Computing Center (HPCC) at Jilin University for computational resources is also acknowledged.

REFERENCES

(1) Burr, G. W.; Shenoy, R. S.; Virwani, K.; Narayanan, P.; Padilla, A.; Kurdi, B.; Hwang, H. Access devices for 3D crosspoint memory. *J. Vac. Sci. Technol. B* **2014**, *32* (4), 040802.
(2) Xia, Q.; Yang, J. J. Memristive crossbar arrays for brain-inspired computing. *Nat. Mater.* **2019**, *18* (4), 309−323.
(3) DerChang, K.; Tang, S.; Karpov, I. V.; Dodge, R.; Klehn, B.; Kalb, J. A.; Strand, J.; Diaz, A.; Leung, N.; Wu, J.; et al. A stackable cross point phase change memory. In *International Electron Devices Meeting (IEDM) Technical Digest*, 2009; pp 1−4.
(4) Ovshinsky, S. R. Reversible electrical switching phenomena in disordered structures. *Phys. Rev. Lett.* **1968**, *21* (20), 1450.
(5) Burr, G. W.; Virwani, K.; Shenoy, R. S.; Padilla, A.; BrightSky, M.; Joseph, E. A.; Lofaro, M.; Kellock, A. J.; King, R. S.; Nguyen, K.; et al. Large-scale (512kbit) integration of multilayer-ready access-devices based on mixed-ionic-electronic-conduction (MIEC) at 100% yield. In *VLSI Symposium on Technology*, 2012; pp 41−42.
(6) Chopra, K. L. Current-controlled negative resistance in thin niobium oxide films. *Proc. IEEE* **1963**, *51* (6), 941−942.
(7) Midya, R.; Wang, Z.; Zhang, J.; Savel'ev, S. E.; Li, C.; Rao, M.; Jang, M. H.; Joshi, S.; Jiang, H.; Lin, P.; et al. Anatomy of Ag/Hafnia-based selectors with 10^{10} nonlinearity. *Adv. Mater.* **2017**, *29* (12), 1604457.
(8) Fazio, A. Advanced technology and systems of cross point memory. In *International Electron Devices Meeting (IEDM) Technical Digest*, 2020; pp 2411−2414.
(9) Jia, S.; Li, H.; Liu, Q.; Song, Z.; Zhu, M. Scalability of sulfur-based ovonic threshold selectors for 3D stackable memory applications. *Phys. Rapid Res. Lett.* **2021**, *15* (6), 2100084.
(10) Wu, R.; Gu, R.; Gotoh, T.; Zhao, Z.; Sun, Y.; Jia, S.; Miao, X.; Elliott, S. R.; Zhu, M.; Xu, M.; Song, Z.; et al. The role of arsenic in the operation of sulfur-based electrical threshold switches. *Nat. Commun.* **2023**, *14* (1), 6095.
(11) Govoreanu, B.; Donadio, G. L.; Opsomer, K.; Devulder, W.; Afanas'ev, V. V.; Witters, T.; Clima, S.; Avasarala, N. S.; Redolfi, A.; Kundu, S.; et al. Thermally stable integrated Se-based OTS selectors with > 20 MA/cm^2 current drive, > 3.103 half-bias nonlinearity, tunable threshold voltage and excellent endurance. In *VLSI Symposium on Technology*, 2017; pp T92−T93.
(12) Cheng, H. Y.; Chien, W. C.; Kuo, I. T.; Yeh, C. W.; Gignac, L.; Kim, W.; Lai, E. K.; Lin, Y. F.; Bruce, R. L.; Lavoie, C.; et al. Ultra-high endurance and low I_{OFF} selector based on AsSeGe chalcogenides for wide memory window 3D stackable crosspoint memory. In *International Electron Devices Meeting (IEDM) Technical Digest*, 2018; pp 3731−3734.
(13) Devulder, W.; Garbin, D.; Clima, S.; Donadio, G. L.; Fantini, A.; Govoreanu, B.; Detavernier, C.; Chen, L.; Miller, M.; Goux, L.; et al. A combinatorial study of SiGeAsTe thin films for application as an Ovonic threshold switch selector. *Thin Solid Films* **2022**, *753*, 139278.
(14) Ravsher, T.; Degraeve, R.; Garbin, D.; Fantini, A.; Clima, S.; Donadio, G. L.; Kundu, S.; Hody, H.; Devulder, W.; Houdt, J. V.Polarity-dependent threshold voltage shift in ovonic threshold switches: challenges and opportunities. In *2021 IEEE International Electron Devices Meeting (IEDM)*, 2021; pp 2841−2844.
(15) Henisch, H. K.; Fagen, E. A.; Ovshinsky, S. R. A qualitative theory of electrical switching processes in monostable amorphous structures. *J. Non-Cryst. Solids* **1970**, *4*, 538−547.
(16) Adler, D.; Shur, M.; Silver, M.; Ovshinsky, S. Threshold switching in chalcogenide-glass thin films. *J. Appl. Phys.* **1980**, *51* (6), 3289−3309.
(17) Ielmini, D.; Zhang, Y. Analytical model for subthreshold conduction and threshold switching in chalcogenide-based memory devices. *J. Appl. Phys.* **2007**, *102* (5), 054517.
(18) Ielmini, D. Threshold switching mechanism by high-field energy gain in the hopping transport of chalcogenide glasses. *Phys. Rev. B* **2008**, *78* (3), 035308.
(19) Jacoboni, C.; Piccinini, E.; Buscemi, F.; Cappelli, A. Hot-electron conduction in ovonic materials. *Solid-State Electron.* **2013**, *84*, 90−95.
(20) Noé, P.; Verdy, A.; d'Acapito, F.; Dory, J.-B.; Bernard, M.; Navarro, G.; Jager, J.-B.; Gaudin, J.; Raty, J.-Y. Toward ultimate nonvolatile resistive memories: the mechanism behind ovonic threshold switching revealed. *Sci. Adv.* **2020**, *6* (9), No. eaay2830.
(21) Liu, J. Microscopic origin of electron transport properties and ultrascalability of amorphous phase change material germanium telluride. *IEEE Trans. Electron Devices* **2017**, *64* (5), 2207−2215.
(22) Karpov, V.; Kryukov, Y.; Savransky, S.; Karpov, I. Nucleation switching in phase change memory. *Appl. Phys. Lett.* **2007**, *90* (12), 123504.
(23) Adler, D.; Henisch, H. K.; Mott, S. N. The mechanism of threshold switching in amorphous alloys. *Rev. Mod. Phys.* **1978**, *50* (2), 209−220.
(24) Buscemi, F.; Piccinini, E.; Vandelli, L.; Nardi, F.; Padovani, A.; Kaczer, B.; Garbin, D.; Clima, S.; Degraeve, R.; Kar, G. S.; et al. A hydroDynamic model for trap-assisted tunneling conduction in ovonic devices. *IEEE Trans. Electron Devices* **2023**, *70* (4), 1808−1814.
(25) Fantini, P.; Polino, N.; Ghetti, A.; Ielmini, D. Threshold switching by bipolar avalanche multiplication in ovonic chalcogenide glasses. *Adv. Electron. Mater.* **2023**, *9* (7), 2300037.
(26) Chen, N.-K.; Wang, B.-Q.; Niu, M.; Sun, H.-B.; Zhang, S.; Li, X.-B. Intensive structural disorder induces electronic delocalization: amorphous solid-liquid transition in ovonic threshold switching Materials. *Adv. Funct. Mater.* **2024**, *34* (52), 2410622.
(27) Jia, S.; Li, H.; Gotoh, T.; Longeaud, C.; Zhang, B.; Lyu, J.; Lv, S.; Zhu, M.; Song, Z.; Liu, Q.; Robertson, J.; Liu, M. Ultrahigh drive current and large selectivity in GeS selector. *Nat. Commun.* **2020**, *11* (1), 4636.
(28) Choi, M.; Sung, H.-J.; Koo, B.; Park, J.-B.; Yang, W.; Kang, Y.; Park, Y.; Ham, Y.; Yun, D.-J.; Ahn, D.; et al. Mechanism for local-atomic structure changes in chalcogenide-based threshold-switching devices. *Adv. Sci.* **2024**, *11* (32), 2404035.
(29) Clima, S.; Matsubayashi, D.; Ravsher, T.; Garbin, D.; Delhougne, R.; Kar, G. S.; Pourtois, G. In silico screening for As/Se-free ovonic threshold switching materials. *npj Comput. Mater.* **2023**, *9* (1), 96.
(30) Clima, S.; Garbin, D.; Opsomer, K.; Avasarala, N. S.; Devulder, W.; Shlyakhov, I.; Keukelier, J.; Donadio, G. L.; Witters, T.; Kundu, S.; et al. Ovonic threshold-switching Ge_xSe_y chalcogenide materials: stoichiometry, trap nature, and material relaxation from first principles. *Phys. Rapid Res. Lett.* **2020**, *14* (5), 1900672.
(31) Li, H.; Robertson, J. A unified mid-gap defect model for amorphous GeTe phase change material. *Appl. Phys. Lett.* **2020**, *116* (5), 052103.
(32) Xu, M.; Xu, M.; Miao, X. Deep machine learning unravels the structural origin of mid-gap states in chalcogenide glass for high-density memory integration. *InfoMat* **2022**, *4* (6), No. e12315.
(33) Konstantinou, K.; Mocanu, F. C.; Lee, T.-H.; Elliott, S. R. Revealing the intrinsic nature of the mid-gap defects in amorphous $Ge_2Sb_2Te_5$. *Nat. Commun.* **2019**, *10* (1), 3065.
(34) Wang, X.-P.; Li, X.-B.; Chen, N.-K.; Chen, Q.-D.; Han, X.-D.; Zhang, S.; Sun, H.-B. Element-specific amorphization of vacancy-ordered GeSbTe for ternary-state phase change memory. *Acta Mater.* **2017**, *136*, 242−248.
(35) Wang, X.-P.; Li, X.-B.; Chen, N.-K.; Chen, B.; Rao, F.; Zhang, S. Phase-change-memory process at the limit: a proposal for utilizing monolayer Sb_2Te_3. *Adv. Sci.* **2021**, *8* (13), 2004185.
(36) Xu, M.; Xu, Q.; Gu, R.; Wang, S.; Wang, C.-Z.; Ho, K.-M.; Wang, Z.; Xu, M.; Miao, X. Tailoring mid-gap states of chalcogenide

Downloaded from pubs.acs.org/jpclcd/article-pdf/17/8/2213/6319089/jz5c03532.pdf by JILIN UNIV, Yu-Ting Huang on 28 October 2026

https://doi.org/10.1021/acs.jpclett.5c03532
J. Phys. Chem. Lett. 2026, 17, 2213−2221

glass by pressure-induced hypervalent bonding towards the design of electrical switching materials. *Adv. Funct. Mater.* **2023**, *33* (45), 2304926.
(37) Konstantinou, K.; Mocanu, F. C.; Akola, J.; Elliott, S. R. Electric-field-induced annihilation of localized gap defect states in amorphous phase-change memory materials. *Acta Mater.* **2022**, *223*, 117465.
(38) Slassi, A.; Medondjio, L.-S.; Padovani, A.; Tavanti, F.; He, X.; Clima, S.; Garbin, D.; Kaczer, B.; Larcher, L.; Ordejon, P.; Calzolari, A. Device-to-materials pathway for electron traps detection in amorphous GeSe-based selectors. *Adv. Electron. Mater.* **2023**, *9* (4), 2201224.
(39) Kresse, G.; Furthmüller, J. Efficiency of ab-initio total energy calculations for metals and semiconductors using a plane-wave basis set. *Comput. Mater. Sci.* **1996**, *6* (1), 15−50.
(40) Kresse, G.; Furthmüller, J. Efficient iterative schemes for ab initio total-energy calculations using a plane-wave basis set. *Phys. Rev. B* **1996**, *54* (16), 11169−11186.
(41) Kresse, G.; Joubert, D. From ultrasoft pseudopotentials to the projector augmented-wave method. *Phys. Rev. B* **1999**, *59* (3), 1758−1775.
(42) Blöchl, P. E. Projector augmented-wave method. *Phys. Rev. B* **1994**, *50* (24), 17953−17979.
(43) Perdew, J. P.; Burke, K.; Ernzerhof, M. Generalized gradient approximation made simple. *Phys. Rev. Lett.* **1996**, *77* (18), 3865−3868.
(44) Hegedüs, J.; Elliott, S. R. Microscopic origin of the fast crystallization ability of Ge−Sb−Te phase-change memory materials. *Nat. Mater.* **2008**, *7* (5), 399−405.
(45) Deringer, V. L.; Tchougréeff, A. L.; Dronskowski, R. Crystal Orbital Hamilton Population (COHP) analysis as projected from plane-wave basis sets. *J. Phys. Chem. A* **2011**, *115* (21), 5461−5466.
(46) Maintz, S.; Deringer, V. L.; Tchougréeff, A. L.; Dronskowski, R. Analytic projection from plane-wave and PAW wavefunctions and application to chemical-bonding analysis in solids. *J. Comput. Chem.* **2013**, *34* (29), 2557−2567.
(47) Maintz, S.; Deringer, V. L.; Tchougréeff, A. L.; Dronskowski, R. LOBSTER: A tool to extract chemical bonding from plane-wave based DFT. *J. Comput. Chem.* **2016**, *37* (11), 1030−1035.
(48) Justo, J. F.; de Brito Mota, F.; Fazzio, A. First-principles investigation of a-SiN:H. *Phys. Rev. B* **2002**, *65* (7), 073202.
(49) Lee, J.; Kim, S.; Lee, S.; Ban, S.; Heo, S.; Lee, D.; Mosendz, O.; Hwang, H. Improving the SiGeAsTe ovonic threshold switching (OTS) characteristics by microwave annealing for excellent endurance and low drift characteristics. In *IEEE Symposium on VLSI Technology Circuits*, 2022; pp 320−321.
(50) Garbin, D.; Devulder, W.; Degraeve, R.; Donadio, G. L.; Clima, S.; Opsomer, K.; Fantini, A.; Cellier, D.; Kim, W. G.; Pakala, M.; et al. Composition optimization and device understanding of Si-Ge-As-Te ovonic threshold switch selector with excellent endurance. In *International Electron Devices Meeting (IEDM) Technical Digest*, 2019; pp 3511−3514.
(51) Chen, N.-K.; Han, D.; Li, X.-B.; Liu, F.; Bang, J.; Wang, X.-P.; Chen, Q.-D.; Wang, H.-Y.; Zhang, S.; Sun, H.-B. Giant lattice expansion by quantum stress and universal atomic forces in semiconductors under instant ultrafast laser excitation. *Phys. Chem. Chem. Phys.* **2017**, *19* (36), 24735−24741.
(52) Emin, D.; Seager, C. H.; Quinn, R. K. Small-polaron hopping motion in some chalcogenide glasses. *Phys. Rev. Lett.* **1972**, *28* (13), 813−816.
(53) Holstein, T. Studies of polaron motion: Part II. The "small" polaron. *Ann. Phys.* **1959**, *8* (3), 343−389.
(54) Nardone, M.; Simon, M.; Karpov, I. V.; Karpov, V. G. Electrical conduction in chalcogenide glasses of phase change memory. *J. Appl. Phys.* **2012**, *112* (7), 071101.
(55) Zhu, M.; Cojocaru-Mirédin, O.; Mio, A. M.; Keutgen, J.; KüPers, M.; Yu, Y.; Cho, J.-Y.; Dronskowski, R.; Wuttig, M. Unique bond breaking in crystalline phase change materials and the quest for metavalent bonding. *Adv. Mater.* **2018**, *30* (18), 1706735.
(56) Kooi, B. J.; Wuttig, M. Chalcogenides by design: functionality through metavalent bonding and confinement. *Adv. Mater.* **2020**, *32* (21), 1908302.
(57) Lee, T. H.; Elliott, S. R. The relation between chemical bonding and ultrafast crystal growth. *Adv. Mater.* **2017**, *29* (24), 1700814.
(58) Lee, T. H.; Elliott, S. R. Chemical bonding in chalcogenides: the concept of multicenter hyperbonding. *Adv. Mater.* **2020**, *32* (28), 2000340.
(59) Luo, Y.; Park, J.; Bernardi, M. First-principles diagrammatic Monte Carlo for electron−phonon interactions and polaron. *Nat. Phys.* **2025**, *21* (8), 1275−1282.
(60) Emin, D. Current-driven threshold switching of a small polaron semiconductor to a metastable conductor. *Phys. Rev. B* **2006**, *74* (3), 035206.
(61) Zhao, Z.; Clima, S.; Garbin, D.; Degraeve, R.; Pourtois, G.; Song, Z.; Zhu, M. Chalcogenide ovonic threshold switching selector. *Nano-Micro Lett.* **2024**, *16* (1), 81.
(62) Fantini, P.; Ghetti, A.; Varesi, E.; Pirovano, A.; Pellizzer, F.; Baratella, D.; Ribaldone, C.; Caravati, S.; Campi, D.; Bernasconi, M.; et al. Microscopic model of the operation of the single-chalcogenide X-point memory. *Commun. Mater.* **2026**, in press, DOI: 10.1038/s43246-025-01044-2

Downloaded from pubs.acs.org/jpclcd/article-pdf/17/8/2213/6319089/jz5c03532.pdf by JILIN UNIV, Yu-Ting Huang on 28 October 2026